NRIAG JOURNAL OF ASTRONOMY AND GEOPHYSICS
2020, VOL. 9, NO. 1, 321–329
https://doi.org/10.1080/20909977.2020.1743914

OPEN ACCESS Check for updates

Analytical investigation for the satellite ranging data of changchun-SLR station

Makram Ibrahim [a], Afaf M. Abd El-Hameed [a], Zhipeng Liang [b] and Xingwei Han [b]

[a]Solar and Space Research Department, National Research Institute of Astronomy and Geophysics (NRIAG), Cairo, Egypt; [b]Satellite Laser Ranging Research Department, Changchun Observatory of National Astronomical Observatories, CAS, Changchun, China

ABSTRACT

In the presented paper, a model describing the range equation, the energy received, the number of returned photons, and photoelectrons as well as the Time-Of-Flight, has been analytically studied. The data concerning the Satellite Laser Ranging (SLR) observed from the Changchun Observatory are considered to evaluate some of the parameters such as the energy received to ground telescope $\mathbf{E_{recv}}$, the number of returned photons $\mathbf{N_p}$ and photoelectrons $\mathbf{N_{pe}}$. The SLR-data are taking into our consideration with the summarised results for the observations taken from the first quarter of 2018. The model is applied on a variety of satellites with different heights and configurations. The results have shown and confirmed the dependency of these parameters on the properties of the laser and detector systems and the used setup.

ARTICLE HISTORY
Received 22 August 2019
Revised 25 February 2020
Accepted 11 March 2020

KEYWORDS
Changchun SLR-station; range correction; analytical model; laser system; returned photons and Photoelectrons

1. Introduction

The ground-based laser ranging is considered to be one of most accurate mechanisms available for tracking satellites (Pearlman et al. 2002). The range describing the distance between the satellite and the tracking station is measured to be half of the measured time multiplied by the speed of light. This technique is used for the satellites with retro-reflectors on their surfaces. These retro-reflectors are assumed to be Lambertian reflectors with a fixed size and a particular reflectivity (Lukesh et al. 2000, 2000). The Changchun-SLR station is one of the international laser ranging systems, so as the Helwan-SLR station (Zhao et al. 2002, Liu 2002, Liu et al. 2004; Ibrahim 2011; Liang et al. 2019). Previously, the laser system and parameters used for ranging and tracking satellites have been studied using Helwan – SLR data (Ibrahim et al. 2011; Matlas et al. 2010; Ibrahim 2011; Ibrahim et al. 2015). In Changchun observatory, the daytime tracking is carried out by updating the original system to adapt the new technology for day-light KHz (Han et al. 2013; Liang et al. 2019). In the range equation, the factor represents the optical cross-section as well as the optical parameters of the reflectors are considered. This equation is useful for the characterisation of the returned signals (Ibrahim and Uozumi 2018).

In the present work, the formulised model represents the parameters corresponding to the range equation, energy photons, returned photon, photoelectrons, etc, are carried out. The equations explained the factors of the range measurement and that of impacting on the received signals quantities are given. The photons returned from the satellite array retroreflectors to the ground telescope are performed to check the essentials of the devices and laser system. The modelling equations are applied on the satellites Starlette, Ajisai, Lageos-1, and Etalon-1 and using the observational satellite ranging data taken from the Changchun-SLR station. These satellites are considered as examples of spherical satellites' shape with different altitudes and sizes. The obtained results are discussed.

2. Changchun SLR-Station

The Changchun SLR-station uses a computer-controlled azimuth and elevation mount for telescope pointing (Liu 2002;, Zhao et al. 2002; Liu et al. 2004). The transmitter is taken to be 20 cm refractor telescope, which the receiver diameter is 60 cm. The type of the detector is a Compensated Single Photon Avalanche Diode (C-SPAD) with quantum efficiency of 20% at 532 nm wavelength. It works in Geiger mode to detect the single-photon echoes (Zhao et al. 2008). The (C-SPAD) system has been made by the Czech Technical University with single-photon sensitivity and 30psec timing precision. The laser generator is an Nd-YAG solid-state Q-switched laser manufactured by photonic industries. The output average energy is 1mJ with pulse width 25 Ps, with the repetition rate 1 kHz at 532 nm of wavelength. The beam divergence is 0.4 mrad, at laser chamber, and directed through cloud paths and compressed to 22 μrad via the transmitting telescope. For environment

CONTACT Afaf M. Abd El-Hameed mostafaafaf2000@yahoo.com National Research Institute of Astronomy and Geophysics (NRIAG), Helwan 11421, Cairo, Egypt

© 2020 The Author(s). Published by Informa UK Limited, trading as Taylor & Francis Group.
This is an Open Access article distributed under the terms of the Creative Commons Attribution License (http://creativecommons.org/licenses/by/4.0/), which permits unrestricted use, distribution, and reproduction in any medium, provided the original work is properly cited.

parameters, MET3 meteorological measurement system manufactured by Paroscientific Inc. is used. It measures atmospheric pressure with a precision up to 0.08 mbar, and temperature to 0.1 degrees Celsius, and measuring relative humidity with1% precision.

2.1. Calibration method used in Changchun SLR-station

The Changchun SLR-station is calibrated with a periscope type device placed in the dome. The device has two diagonal reflectors to make a U-shape optical path to connect transmitter and receiver telescopes. When calibration is started, the telescope is turned to preset coordinate, and an iris is placed in the laser beam to weaken beam energy. The laser beam propagates through the periscope, enters receiving aperture and triggers echo signal. The calibration constant is computed to be the average of nearly 5000 returns (echoes). Figure 1(a) shows the histogram of the calibration which carried out on 10 July 2018. The mean value of the calibration is 209,725.8 ps, while Root Mean Square (RMS) is 90.2 ps. In the plotted Figure 1(b), the solid line specifies the mean, while dotted line specifies the ± RMS.

2.2. Range correction due to the atmospheric effects at the Changchun-SLR Station

The range correction resulted from the atmospheric effect is calculated using the Marini-Murray model (Marini and Murray 1973). This requires taking the local atmospheric measurements at the ranging location. The Changchun station observations are taken at elevation 10° degrees. The Marini-Murray model is carried out to compute the correction in the range of the satellite. The model is applied at the same meteorological condition during the observation of the satellite Starlette which is observed on January 1st, 2018, and the results are shown in Figure 2. The factor R_H is the relative humidity, λ is the wavelength, T is the temperature and P_0 is the atmospheric pressure. The symbol φ is the latitude of the station and HH is the station height above the mean sea level. All of these parameters are measured at the location of the station. The results have shown the correction of the range is about 2.413 m at the elevation angle 90° degrees. This value is reached to 6.997 m at 20° degrees. As for the Helwan-SLR station, it increases to about 13.432 m at the elevation angle of 10° which is the minimum elevation angle at the Changchun-SLR station.

3. Analytical model

3.1. The range equation

In the laser for the satellite ranging, the equation describing the range equation is used to estimate the returned photons. Some of the parameters such as the power and energy of the laser system, the diameters of the receivers, as well as the effects of the atmosphere are taken into consideration in the range equation. This equation is used to predict the laser system performance (Lukesh et al. 2000, 2001). Accordingly, the formula of the received energy $\mathbf{E_{recv}}$ can be written in the simple form as:

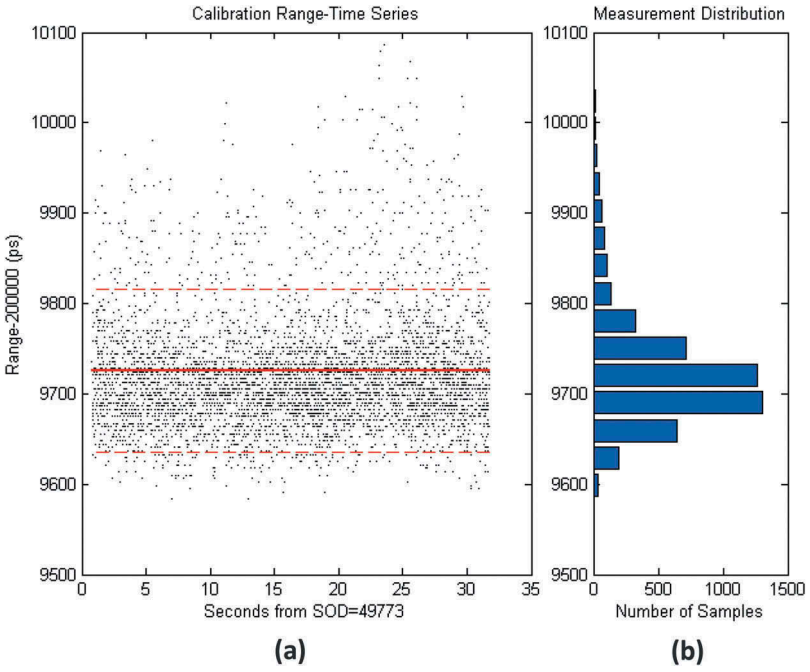

Figure 1. Sample of calibration. Measurement time series is shown as in (a), mean of measurement is specified with a solid line, and root mean square of the session is depicted with two dashed parallel lines around the mean. The histogram of the measurement is shown in (b).

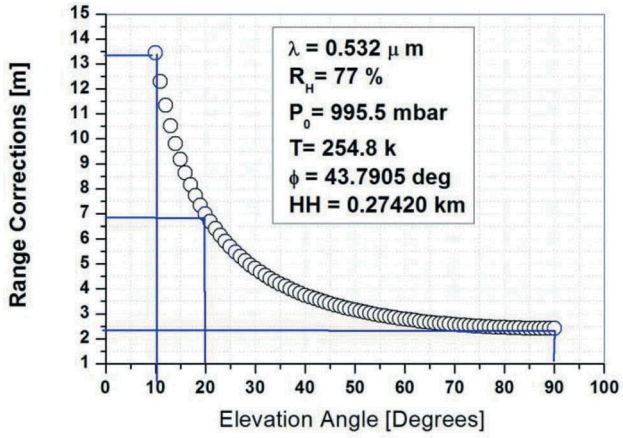

Figure 2. Range correction as computed for the parameters obtained on 1 January 2018 at the Changchun-SLR station.

$$E_{recv} = P_{out} \times P_{in} \times \sigma = \frac{D_T^2 E_T}{\lambda^2 R^2} \tau_{trans} \tau_{atm} \times \frac{A_T}{R^2} \tau_{recv} \tau_{atm} \times \sigma \quad (1)$$

With $$\sigma = \rho A_{cc} \left(\frac{4\pi}{\Omega}\right) \times \frac{N_{CC}}{2} = \rho A_{cc} \left(\frac{4\pi A_{cc}}{\lambda^2}\right) \times \frac{N_{CC}}{2}$$

where P_{out} and P_{in} are the extrinsic path from the transmitter to the satellite and the internal path from the satellite target to the grounded receiver, respectively, and σis the optical cross-section (Degnan 1985; Lipinski et al. 1994). D_T, diameter of the transmitter, E_T' the energy of the transmitted pulse, R is the range to the satellite, τ_{trans} is the losses term, and τ_{atm} is the atmospheric transmission to satellite. The term A_T is the collecting area of the receiver, τ_{recv} is the losses from the effects of the optical transmission and detector. ρ, is the target reflectivity, A_{cc} is the light-collecting area of the corner cube object. The on axis retroreflector gain is $\frac{4\pi}{\Omega}$ in which Ω is the effective solid angle occupied by the far-field diffraction pattern of the retroreflector. For several retro-reflectors, N_{CC} is the optical cross-section of the satellite, which can be computed by summing the contributions of the total number of retroreflectors (Lipinski Ronald et al. 1994). The satellites are chosen to have the spherical shape, to keep away from the large pulse dispersion which can be caused by plane array panels when it is sighted at non-normal incidence. For circular access hole, the far-field diffraction pattern is the Airy pattern (Born and Wolf 1975, and Ibrahim et al. 1997). The characteristics of the spherical satellites with different altitude and heights, and considered in this study are given in Table 1. For longer slant ranges, more retroreflectors are required to achieve reasonable signal-to-noise ratios.

3.2. Returned photons

The returned photons N_P as collected at the surface of receiver can be formularised through the relation in equation (3) as (Degnan 1985; Lipinski Ronald et al. 1994);

$$N_P \approx \frac{4\pi I \tau_{lp} N_{cc} T_v \cos(\theta) r_{cc}^2 r_t^2 \lambda}{h c \theta_{LRA}^2 R^2} \quad (3)$$

where I is the laser beam intensity on the target, τ_{lp} is the laser pulse length, N_{cc} is the number of the retroreflector corner cubes on the satellite that facing the beam, T_v is the fraction of beam energy transmitted through the atmosphere vertically, θ is the beaming angle off vertical which can be defined as the angle between the elevation value and zenith, r_{cc} is the radius of retroreflector corner cubes, r_t is the radius of the receiving telescope, λ is the wavelength, h is Planck's constant, c is the speed of light, and θ_{LRA} is the full angle divergence from the corner cubes.

3.3. Photoelectrons

According to the Radar link equation, the number of photoelectronsN_{pe}can be evaluated. This is given by the following formula (Degnan 1985);

$$N_{pe} = \eta_q E_T \frac{\lambda}{hc} \eta_T G_T \sigma \left(\frac{1}{4\pi R^2}\right)^2 A_T \eta_R T_A^2 T_C^2 \quad (4)$$

Table 1. Characteristics for some spherical satellites.

Sat. Name	Cosper ID	Hight [km]	σ [m^2]	Diameter of satellite [m]	No. of retroreflectors	Sat. shape
Starlette	7501001	950	0.65	0.24	60	sphere
Ajisai	8606101	1400	12	2.15	1436	sphere
Lageos-1	7603901	6000	7	0.60	426	sphere
Etalon-1	8900103	19,000	60	1.294	2146	sphere

where η_q is the quantum efficiency of the photomultiplier, η_R and η_T are the received and transmitted path efficiency. The values of T_A and T_C are the transmission properties of the atmosphere and the circus cloud. The other parameters are defined and given above. The symbol G_T is the transmitter gain which defined from the Gaussian beam as in the relation (Degnan 1985);

$$G_t(\theta) = \frac{8}{\theta^2}\exp\left[-2\left(\frac{\theta_P}{\theta_t}\right)\right] \quad (5)$$

whereθ_t, is the far-field divergence half-angle with the $\mathbf{1/e^2}$ intensity point. θ_P is the beam pointing error. To determine the gain of the transmitter, the value of θ_P is often replaced by θ_t. So, the transmitter gain can become $8/\theta_t^2$.

3.4. Signal to noise ratio

The total noise is mainly depending on the change in repetition rate because of detector dark noise and laser back scatter noise. The detector dark counts can be often reduced by cooling the detector. The detector types have higher quantum efficienciesη_q (40% to 55%) at the 532 nm SLR wavelength; will allow higher noise to be entered into the detector during the day time (Degnan 2008). For laser back scatter noise, when satellite ranging, there are repeated periods of overlaps between returning photons, and just fired laser shots. The backscatter of these shots from the first few km travelling through the troposphere – would cause significant noise on the single photon-diode, reducing the detection probability for the return photon. This type of degradation of return signal is called laser backscatter noise. This situation can be avoided through the implemented of the system within an FPGA (Field Programmable Gate Array) device, but would achieve only resolutions of 100 ns (10 MHz); to improve the resolution, a programmable, analogue delay generator covers an additional resolution of 0–100 ns, thus increasing the resolution to <0.5 ns (Iqbal et al. 2008). On the other hand, the increasing of the energy will increase the laser backscatter noise and increasing the repetition rate will decrease the energy per pulse concludes that at higher repetition rate backscatter will occur more frequently but due it will be less intense (Iqbal 2011, and Hampf et al. 2019). Signal to noise ratio of almost all the satellites follow the behaviour of the curve shown in Figure 3.

Tracking the low altitude satellites with higher repetition rate has obvious advantages due to higher achieved signal-to-noise ratio. In case of high altitude satellites, very low values for the signal-to-noise ratio would be obtained. This is due to the signal is dropped by a factor of the power four. For low altitude satellites, and from the signal-to-noise ratio depicted as Figure 3, there are significant increases in signal due increase of repetition rate, i.e. 10–100 K pulses per second as compared to 2 K pulses, but the increase in signal-to-noise ratio is not so linearly (2296.08 at 10 kHz as compared 1189.43 at 2 kHz) because of the increase in the repetition rate decreases the pulse energy. Moreover, signal-to-noise ratio is decreased because of the increase in the dark noise with higher repetition rate and laser backscatter starts to contribute a significant amount of noise at the value 10 kHz and higher.

3.5. Probability of the detected photoelectrons

To carry out the mean number of photoelectrons, the probability $P_d$of a particular outgoing pulse yielding detected returned photoelectrons $N_{pe}$is considered. This factor is proportional to the values of N_{pe} through the relation (Degnan 2017);

$$P_d(N_{pe}) = 1 - \exp(-N_{pe}) \quad (6)$$

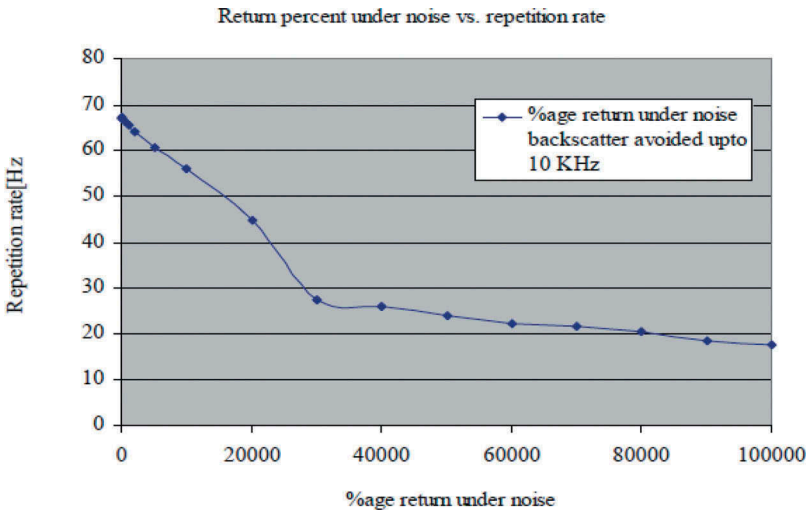

Figure 3. Percentage return under noise (Iqbal 2011).

Accordingly, this value is tended towards one at high mean photoelectrons per pulse.

3.6. Time-of – flight

In satellite laser ranging, the measurement of the time required for a laser pulse to be radiated towards satellites and space objects in the sight and returning back to a detector is expressed as the time-of-flight (TOF). The TOF is usually derived from the Consolidated Prediction Format (CPF) predictions available from the ILRS website (ILRS: Consolidated prediction format, 2018). This format accurately predicts positions and ranges for variety of laser-ranging targets. The TOF is based on the photon counting to perform the measurements, and may be used to enhance the accuracy of the tracked satellites (Lussana et al. 2015; Hampf et al. 2019). The TOF can be estimated using the range of the target and the speed of light. This is given as the following formula (Hampf et al. 2019);

$$\mathrm{TOF} = \frac{2\ \mathrm{R}}{\mathrm{C}} \tag{7}$$

The modelled equations are applied on the satellites motioned in Table 1. The laser system parameters and the used conditions taken from the Changchun-SLR station are summarised in Table 2. In this study, for simplicity, the weather and cloudy conditions are estimated to be good visibility conditions, and in this case, the transmission properties of the circus cloud $\mathbf{T_c}$ is considered to be equal one (Marini and Murray 1973).

4. Results and Discussion

The computational results are applied for some spherical satellites with different configurations and ranges such as those of the satellites Starlette, Ajisai, Lageos-1 and Etalon-1 as given in Table 1. The obtained relations and results of the applied model are discussed in detail as follows;

Table 2. The estimated properties of the system and laser parameters of the Changchun-SLR station.

Parameters	Value
Wavelength, λ	0.532 μm
Energy of laser pulse, E_{tran}	1 mJ
Photo energy at working wave length, E_{Ph}	~ 3.74 x 10^-19 J
Pulse width	25 Psec
Repetition rate	1 KHz
(At Tx aperture) transmission beam divergence θ_t	22 μrad
Transmitted aperture dimension (diameter), D_T	200 mm
Receiver diameter, D_R	60 cm
Transmission efficiency, K_T	0.8
Transmission efficiency of corner cubes, K_{LRA}	~ 0.9
Receiving efficiency, K_R	0.5
Atmospheric transmission efficiency, T	~ 0.7
Target reflectivity, ρ	0.9
Beaming angle off vertical, θ	45°
Full angle divergence from the corner cubes, θ_{LRA}	0.1 mrad
Effective diameter of the retroreflector array, D_{LRA}	~ 3 cm
Detector quantum efficiency, η_q	20%

(a) The satellite Starlette

Figure 4(a) clarifies the relation between the range and the energy reached at the surface of the grounded receiver telescope as computed for the satellite Starlette. The data are plotted at different times of laser shots. It is clear from the figure that the satellite rang is decreasing with the increase of the returned energy. This is agreeing well with equation (1) as a result of R^4effect (Makram Ibrahim et al. 2011). The small values of the returned energy are dependent on the dimension of the surface of the ground telescope. Figure 4(b) is plotted to obtain the relationship between the numbers of the received photons $\mathbf{N_p}$ and the returned photoelectrons $\mathbf{N_{pe}}$. The values of these two parameters are produced using the (C-SPAD) which has a quantum efficiency of 20%. This figure shows that Np and Npe have the same behaviour as both are increasing with the increasing of the elevation angle and vice versa. It is also clear that the number of photons is usually higher than the number of photoelectrons.

(b) The satellite Ajisai

Figure 5(a,b) is plotted for the data results obtained for the satellite Ajisai. Figure 5(a) clarifies the relations between the satellite ranges versus the energy received to the telescope. The data are plotted at different times of observation. The number of returned photons and photoelectrons is shown in Figure 5(b). The figures show the same behaviour obtained in the case of the satellite Starllette.

The figures clarify that the values of the energy received from the satellite Ajisai are higher than that obtained from the satellite Starlette, which is considered as the lower one. The reason is referred to what is the so-called satellite signature (Appleby 1992, and Hanna et al. 2012). Also, the type of retroreflectors, their numbers as well as their orbital trajectory is varied significantly from satellite to another. This leads to different optical responses in which Ajisai has the most favourable one (Villoresi et al. 2008). Ajisai is an example of high signature satellites and Starlette is an example for low signature satellites. It is known that as the array of corner cubes reflectors increases on the satellites, the possibility to obtain a large amount of range data increases also.

(c) The satellite Lageos-1

Figure 6(a,b) clarifies the data resulted for the satellite Lageos-1, in which the relations are plotted at different times of laser shots. The graphs confirm the same behaviour obtained in the above two satellites and discussed before in Figures 4, 5.

(d) The satellite Etalon-1

The satellite Etalon-1 is a passive geodetic satellite dedicated to satellite laser ranging. It contains only instrumentation of retro-reflector array that consists of two

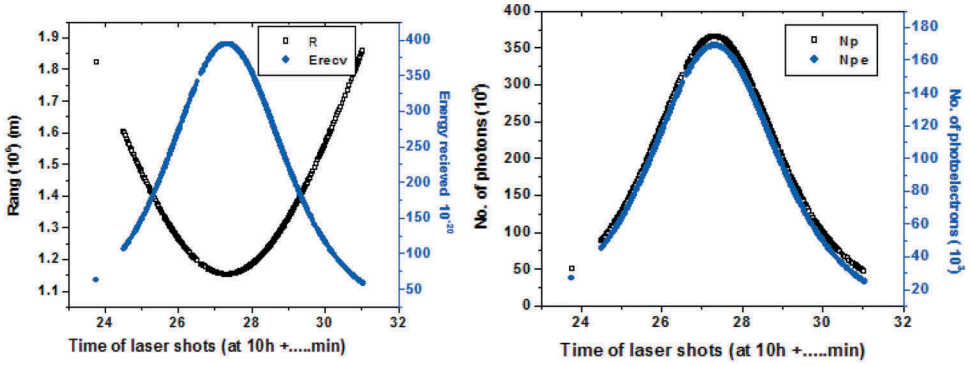

(a) (b)

Figure 4. The satellite Starlette, (a): the range R versus received energy E_{recv} and (b): Np versus Npe.

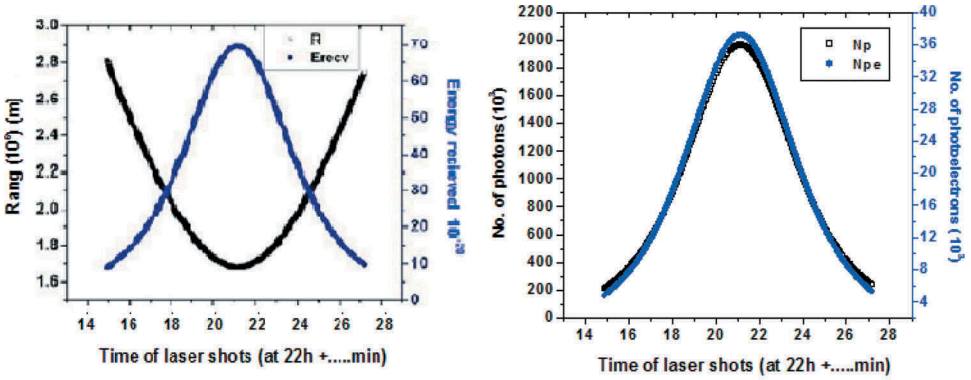

(a) (b)

Figure 5. The satellite Ajisai, (a): the range R versus received energy E_{recv} and (b): Np versus Npe.

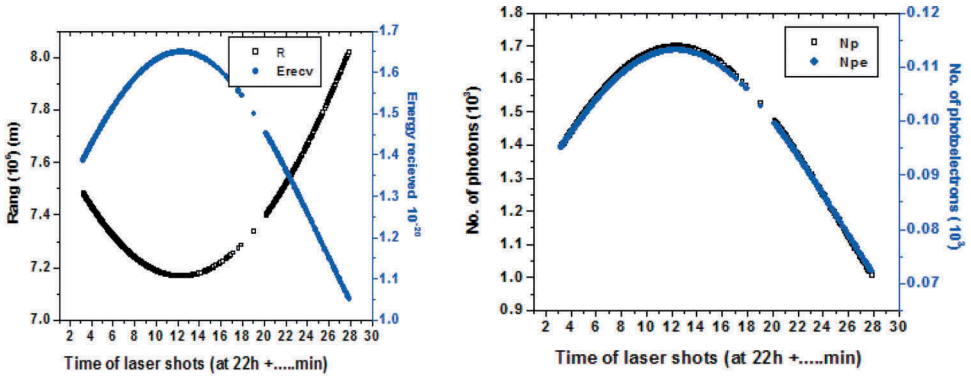

(a) (b)

Figure 6. The satellite Lageos, (a): the range R versus received energy E_{recv} and (b): Np versus Npe.

different types of corner cubes. The orbit of this satellite is circle with period 11 h and 16 min. Figure 7(a,b) clarify the same relations plotted in the other satellites considered in this study. The figures show almost the same trend obtained above.

It is noticed here that, for the same energy of laser pulses, the received energy values are dependent on the satellite properties representing the number of retro-reflectors and satellite range as well. In addition, the obtained values of the parameters, representing the number of returned photons and photoelectrons of this satellite, are smaller in comparable with that obtained for the other satellites. This is due to the satellite Etalon has the highest range.

Comparing with the results obtained from studying of these parameters using the Helwan-SLR observation, it must notify here that the $\mathbf{N_p}$ and $\mathbf{N_{pe}}$ values obtained from the Changchun – SLR are smaller than that obtained from Helwan station. This is due to the less value of the energy for the used laser pulses. In addition, the satellite Etalon-1 cannot be observed from Helwan-SLR station because of the laser system

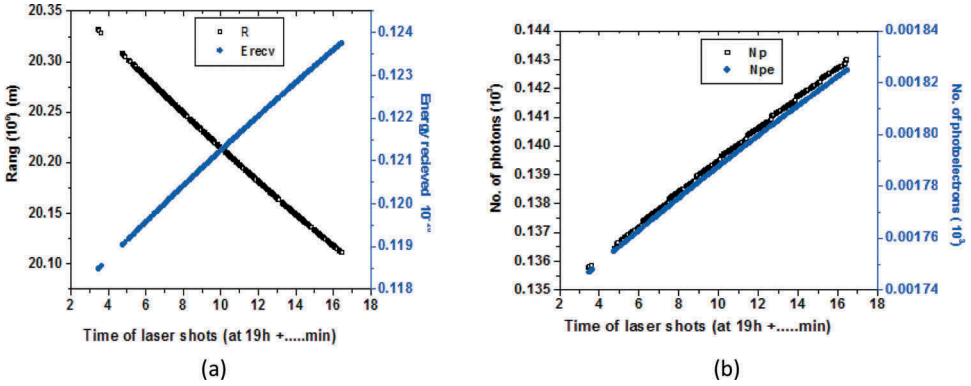

Figure 7. The satellite Etalon-1, (a): the range R versus received energy E_{recv} and (b): Np versus Npe.

at Helwan is not enough to reach the satellites of higher altitudes and range.

On the other hand, the probability concerning the average of the detected photoelectrons is carried out for the four satellites considered in the analysis. For this purpose, Figure 8 clarifies the probability factor $P_d\,(N_{pe})$as a function of the detected photo-electronsN_{pe}. It is noticed from the figure that, for all satellites except the satellite Etalon-1, the values of P_d are approximately closed to be equal one. This is shown in Figure 8(a-c) for the satellites Starlette, Ajisai, and Lageos respectively. This result confirms the high values of the detected photoelectrons with a very small difference in the obtained P_d data for the considered three satellites. On contrary, for the satellite Etalon-1 shown as Figure 8(d), the different behaviour is observed. The values of P_d are increased until reaching the maximum value, and is found to be less than one. This result confirms the lower values for the detected photoelectrons of this satellite.

The time-of-flight TOF is estimated and evaluated using the range of the satellites. This factor indicates the accuracy of the predictions for the tracked targets. The TOF data are plotted for the four satellites and shown in Figures (9a-d) respectively. The figures show the same behaviours for all the four satellites, in which the "TOF" value is increasing with the range.

For the satellite Etalon-1 of the higher considered range, and seen in Figure 9(d), the TOF values are observed to be the highest one. The maximum values of the "TOF" for all satellites are given in Table 3.

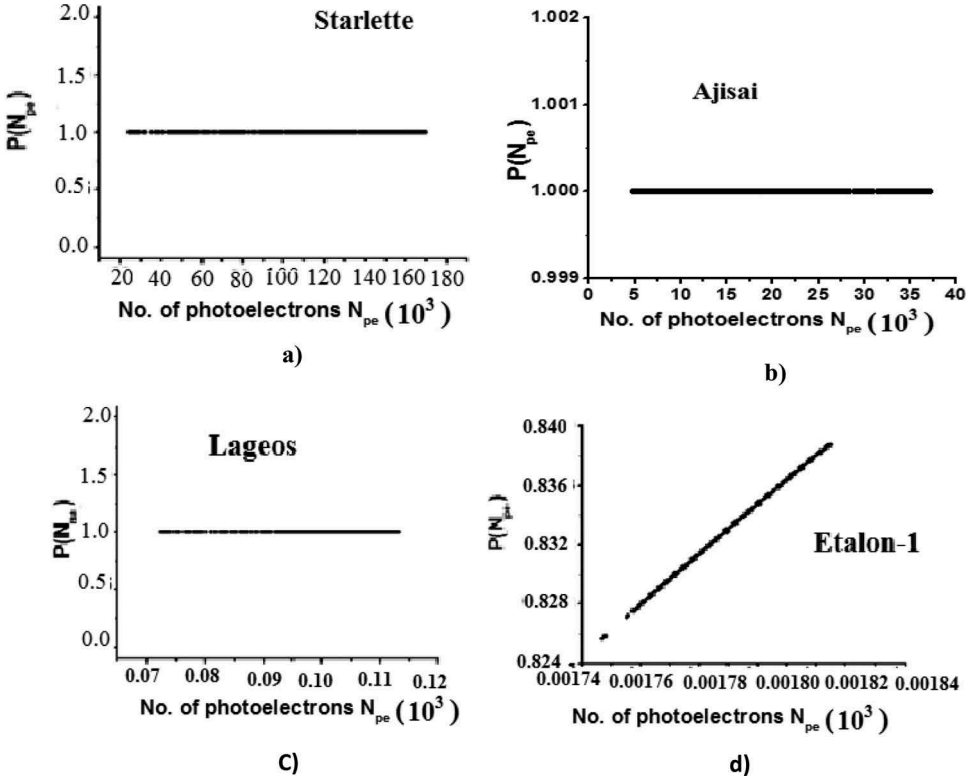

Figure 8. Probability values of the detected photoelectrons for the satellites.

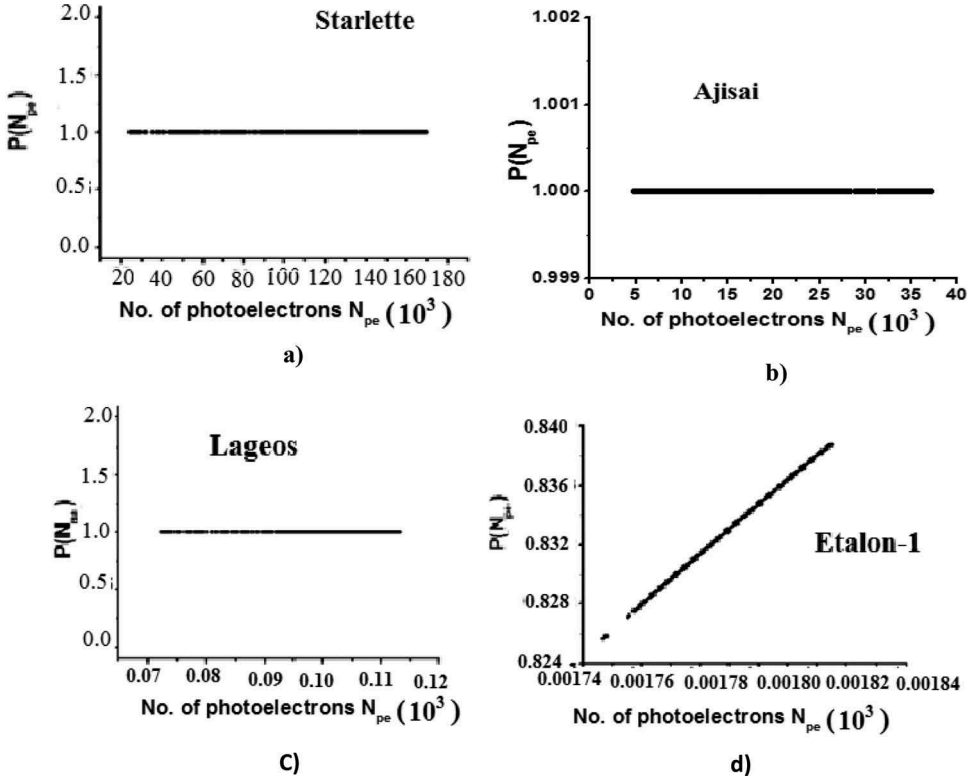

Figure 9. TOF data versus the satellite range.

Table 3. Maximum TOF values.

Satellite	Maximum range (R_{max}) x 10^6 (m)	Time-of-flight TOF (ms)
Starlette	1.86564	12.44
Ajisai	2.81276	18.75
Lageos	8.02499	53.5
Etalon-1	20.33148	135.54

5. Conclusion

In this research, the ground-based laser for ranging satellites from Changchun-SLR station has been analytically studied. The Marini-Murray model is used for computing the atmospheric effect on the range at different elevation angles. It shows that the correction in the range is nearly 2.143 m at the elevation angle 90°, and increased to be about 13.432 m at the minimum elevation angle of 10°. The analytical model representing the range equation has been studied using the parameters of laser systems and the atmospheric conditions of the used satellites. The formulas are applied on some spherical satellites with different heights. These satellites are Starlette, Ajisai, Lageos-1, and Etalon-1, which have been observed from the Changchun-SLR station during the first quarter of 2018. The results show that the factors describing the transmission and receiver setup as well as the laser parameters, are more efficient for determining the number of returned photons and the number of photoelectrons as well. It is evidence that the data plotted for the number of returned photons N_p and the photoelectrons N_{pe} have the same behaviour at different times of laser shots, with N_p is usually higher than N_{pe}. Due to the highest range of satellite Etalon-1, the values of the obtained data of this satellite are smaller in comparable with that obtained for the other satellites and resulted in the lower numbers of N_p and N_{pe}. On the other hand, the probability concerning the average of the detected photoelectrons is evaluated, and the results show the less values of the satellite Etalon-1, because it is the highest altitude satellite from the used samples. The time of flight "TOF" is also computed for the considered satellites and the values obtained for the satellite Etalon-1s the greatest one.

We would like to reveal that in the previous work we used the data from the Helwan SLR station. The laser system in Helwan cannot reach to the high orbit satellites such as Etalon-1 (20 thousand km). In addition to that we concluded that the two main parameters required for the laser to reach the high altitude satellites (such as Etalon-1) are the diameter of the receiver of the telescope to be large enough and the divergence angle of the laser to be narrow in the order of μrad. In this work, we confirm our previous conclusion by using the small divergence angle (22 μrad) and also the great size for the diameter of the telescope (60 cm) as used in the Changchun SLR station.

Article highlights

(1) SLR-data are taken from the Changchun station with the summarized results for the first quarter of the 2018.

(2) An analytical model describing the received energy, the number of returned photons, the number of photoelectrons as well as the Time –Of-Flight "TOF" is studied.
(3) The model is applied to a variety of satellites with different heights and configurations.
(4) The obtained results are discussed.

Disclosure statement

No potential conflict of interest was reported by the authors.

ORCID

Makram Ibrahim http://orcid.org/0000-0002-7730-4825
Afaf M. Abd El-Hameed http://orcid.org/0000-0003-3666-3132
Zhipeng Liang http://orcid.org/0000-0002-8785-7642

References

Appleby GM. 1992. Satellite signatures in SLR observations. Proc., 8th International Workshop on Laser Ranging Instrumentation, Annapolis, Maryland. 2.1-2.14.

Born M, Wolf E. 1975. Principles of optics. Chapter 8. New York: Perggamon Press.

Daniel H, Ewan S, Fabian S. Otsubo T, Wagner P, Riede W. 2019. Satellite Laser Ranging at 100 kHz pulse repetition rate. CEAS Space J. Published Online doi:10.1007/s12567-019-00247-x.

Degnan JJ. 1985. Millimeter Accuracy Satellite Laser Ranging: A Review. AGU Geodynam Ser. vol. 25. Berlin: Springer; p. 133–162.

Degnan JJ 2008, "Impact of receiver dead time on photon-counting SLR and altimetry during daylight operations", 16th International Laser Ranging Conference, Poznan Poland.

Degnan JJ, 2017, "Challenges to achieving millimeter accuracy normal points in conventional multi- photon and kHz single photon SLR SYSTEMS", In Proceedings of the ILRS Technical Workshop, Riga, Latvia.

Hampf D, Schafer E, Sproll F, et al. 2019. Satellite laser ranging at 100 khz pulse repetition rate. CEAS Space J. 11:363–370.

Han X, Dong X, Song Q, Zhang H, Shi J. 2013. Fulfillment of KHz SLR daylight tracking of Changchun Station, In: Proc. of 17th International Laser Ranging Workshop, Fujiyoshida, Japan; Nov 11 –15.

Hanna YS, Ibrahim M, Wassem Sam SW. 2012. Spline and overlap techniques for analyzing slr data. Space Res J. 5 (1):1–9. doi:10.3923/srj.2012.1.9.

Ibrahim M. 2011. 17 years of ranging from the Helwan-SLR station. Astrophys Space Sci J. 335(2):PP.PP.379–387. doi:10.1007/s10509-011-0741-7.

Ibrahim M, Hanna YS, Samwel SW, Hegazy M. 2015. Satellite laser ranging in Egypt. NRIAG J Astron Geophy. 4(1):123–129. doi:10.1016/j.nrjag.2015.06.002.

Ibrahim M, Uozumi J. 2018. Three-dimensional correlation properties of speckles produced by diffractal-illuminated diffusers. Asian J Phy. 27:457–466. 9-12.

Ibrahim M, Uzumi J, Asakura T. 1997. On the generation of clustered speckle due to ring-slit illumination. Optik. 106:33–41.

IIbrahim M, Abd El-Hameed AM, Attia GF. 2011. Analytical studies of laser parameters for ranging and illuminating satellites from h-slr station. Space Res J. 4(2):71-78.

ILRS. 2018. consolidated prediction format. Accessed Oct 2018. https://ilrs.cddis.eosdis.nasa.gov/data_and_products/formats/cpf.html

Iqbal F. 2011. Investigations and Design Solutions of a High Repetition Rate Satellite Laser Ranging (SLR) System, PhD Thesis, at the Institute for Broadband Communication in co-operation with Observatory, Lustbuhel

Iqbal F, Kirchner G, Koidl F. 2008. Fast response, medium resolution digital event timer and range gate generator for satellite laser ranging. Artificial Satell. 43(4):143–149. doi:10.2478/v10018-009-0013-8.

Liang Z, Dong X, Ibrahim M, Song Q, Han X, Liu C, Zhang H, Zha G. 2019. Tracking the space debris from the Changchun Observatory. Astrophys Space Sci. 364 (11):201. doi:10.1007/s10509-019-3686-x.

Lipinski RJ, Meister DC, Tucker SD, Fugate RQ, Leatherman P, Maes CF, Joseph Lange W, Cowan WD, Meulenberg A, Cleis RA, et al. 1994. Laser beaming demonstrations to high orbit satellites, Proc. SPIE Vol. 2121, p. 222–231.

Liu C. 2002. Performance and observation summary of changchun satellite laser ranging station. Chinese Science Bulletin. 47(13):1070–1072. doi:10.1360/02tb9240.

Liu C, Zhao Y, Fan C et al. 2004. The performance of changchun satellite laser ranging station. Proceeding of 14th International Laser Ranging Workshop, San Fernando, Spain. p.175–177.

Lukesh GW, Chandler SM, Voelz DC. 2000. Estimation of laser system pointing performance by use of statistics of return photons. Appl Opt. 39:1359-1371.

Lukesh GW, Chandler SM, Voelz DC. 2001. Analysis of satellite laser optical cross sections from the active imaging testbed. Proceedings of the 4th EOS/SPIE Symposium on Remote Sensing Optics in Atmospheric Propagation and Adaptive Systems, Jan. 29, European Optical Society. p. 24-33.

Lussana R, Villa F, Mora AD, Contini D, Tosi A, Zappa F. 2015. Enhanced single-photon time-of- flight 3D ranging. Opt Express. 23(19):24962–24973. doi:10.1364/OE.23.024962.

Marini JW, Murray CW, 1973. correction for laser range tracking data for atmospheric refraction at elevations above 10 degrees. NASA, report X-591-73-351. Godard Space Flight Center.

Matlas P, Blaze J, Ibrahim M, Khalil KI, Hanna YS. 2010. Diagnostic improvement of laser system at NRIAG SLR Station in Helwan. NRIAG J Astron Astrophy. 435–444, Special Issue.

Pearlman MR, Degnan JJ, Bosworth JM. 2002. The international laser ranging services. Adv Space Res. 30 (2):135–143.

Villoresi P, Jennewein T, Tamburini F, Aspelmeyer M, Bonato C, Ursin R, Pernechele C, Luceri V, Bianco G, Zeilinger A, et al. 2008. Experimental verification of the feasibility of a quantum channel between space and Earth. New J. Phys. 10 033038.

Zhao Y, Fan CB, Han X, Zhao G, Zhang Z, Dong X, Zhang HT, Shi JY, 2008. Progress in Changchun SLR. Proceedings of the 16th International Workshop on Laser Ranging, Poznan, Poland, pp. 525–530.

Zhao YZ, Fan C, Liu C, Han X, Shi J, Zhang X, Zhang H, 2002. System stability improvement of changchun SLR. Proceedings of 13th International Workshop on Laser Ranging. USA.